Noise studies with Crab Cavities in the SPS for the HL-LHC project

UNIVERSITY OF LIVERPOOL

Thesis submitted in accordance with the requirements of the University of Liverpool for the degree of Doctor in Philosophy

by

Natalia Triantafyllou

Day Month Year

Abstract

Acknowledgments

List of Figures

List of Tables

List of Symbols

E_b	Energy
f_{rev}	Revolution frequency
V_{RF}	Main RF voltage
f_{RF}	Main RF frequency
CC	Crab Cavity
V_{CC}	CC voltage
f_{CC}	*CC* frequency
ϕ_{CC}	*CC* phase
Q_x	Horizontal tune
Q_y	Vertical tune
Q_s	Synchrotron tune
β	Relativistic beta
γ	Relativistic gamma (Lorenz factor)
N_b	Bunch intensity i.e. number of particles (here protons)
Q'_x	Horizontal first order chromaticity
Q'_y	Vertical first order chromaticity

Contents

1 | Introduction

This is the introduction of my PhD thesis.

1. Introduction

In 2018, two prototype Crab Cavities (CCs) were installed in the SPS to be tested for the first time with proton beams. A series of dedicated machine developemnt studies was carried out in order to validate their working principle and answer various beam dynamic questions. One of the operational issues that needed to be addressed concerned the expected emittance growth due to noise in their RF system, which is the main subject this thesis. As mentioned in chapter 3 a theoretical model had already been developed and validated by trackig simulations [1]. As a part of the first experiemental campaign with CCs in SPS a dedicated experiment was conducted to benchmark these models with experimental data and confirm the analytical predictions. The objective of this chapter is to provide an overview of the machine setup for the CC experiements and introduce the instruments and methods used for measuring the beam parameters of interest for the emittance growth studies.

2 | Basics of accelerator beam dynamics

For a gaussian beam distribution the normalised beam emittance is defined as:

$$\epsilon_x = \frac{\sigma_x(s)^2 - \delta^2 D_x^2(s)}{\beta_x(s)} \beta\gamma \tag{2.1}$$

where $\sigma_x(s)$ is the beam size, $\beta_x(s)$ is the beta function, $D_x(s)$ is the dispersion fat a specific location s along the accelerator, $\delta = \Delta p / p0$ is the momentum spread and β, γ the relativistic parameters. Similar expression is valid for the vertical plane, with the difference that there is no dispersion.

3 | Theory of Crab Cavity noise induced emittance growth

4 | Experimental studies 2018: Operational setup and beam instrumentation

The theoretical model for the transverse emittance growth caused by amplitude and phase noise in a CC was introduced in Chapter 3. In 2018, a dedicated experiment was conducted in the SPS to benchmark this model against experimental data and confirm the analytical predictions. In this chapter, the machine setup, the beam configuration and the instrumentation used for the emittance growth studies with CCs in the SPS are presented.

The chapter is structured as follows: Section 4.1 describes the experimental machine configuration. Thereafter, Section 4.2 elaborates on the installation and the operational aspects of the CCs in the SPS. In Sections 4.3- 4.5 the instruments used for the parameters of interest (see Chapter 3, Eq....) i.e. CC voltage, emittance and bunch length are discussed, including the post processing methods where it was performed by the author.

4.1 Machine and beam configuration

For studying the long-term emittance evolution a special mode of operation was set up in the SPS which is called "coast" with bunched beams. In this mode, the bunches circulate in the machine at constant energy for long periods, from a few minutes up to several hours, similar to the HL-LHC case.

To make sure that the SPS can be used as a testbed for the emittance growth studies with CCs an extensive preparatory campaign was carried out through 2012-2017 [2, 3, 4]. The primary concern was the natural emittance growth that was observed

5

in the machine (without noise), as this needs to be well characterized and be kept sufficiently small in order to distinguish and understand the contribution from the CC noise. From these studies, it was concluded that the optimal coast setup is at high energies, with low chromaticity and bunches of low intensity as it minimises the natural emittance growth. The highest energy for which the SPS could operate in "coast" was found to be at 270 GeV and thus the experiments were performed at this energy. Moreover, as the natural emittance growth was found to be a single bunch effect four bunches (the number of bunches was chosen arbitrarily) were used to reduce the statistical uncertainty of the measurements.

During the experiment the Landau octupoles were switched off. Nevetherless, a residual non-linearity was present in the machine mainly due to multipole components in the dipole magnets [5, 6]. Last, the transverse feedback system was switched off. The main machine and beam parameters used in the experiment of 2018 are listed in Table 4.1. It should be noted, that no measurements of chromaticity are available from the day of the experiment. However it was ensured that the chromaticity was corrected to small positive values.

Table 4.1: Main machine and beam parameters for the emittance growth studies with CCs in SPS in 2018.

Parameter	Value
Beam energy, E_b	270 GeV
Revolution frequency, f_{rev}	43.375 kHz
Number of proton per bunch, N_b	3×10^{10} p/b
Number of bunches	4
Bunch spacing	524 ns
Main RF frequency, f_{RF}	200.39 MHz
Main RF voltage, V_{RF}	3.8 MV
Horizontal / Vertical betatron tune, Q_x / Q_y	26.13 / 26.18
Horizontal / Vertical first order chromaticity, Q'_x / Q'_y	~ 1.0 / ~ 1.0
Synchrotron tune, Q_s	0.0051

4.2 Crab Cavities in the SPS

For the SPS tests two prototype CCs of the Double Quarter Wave (DQW) type, CC1 and CC2, were fabricated by CERN and were assembled in the same cryomodule, shown in Fig. 4.1 [7]. The cryomodule was installed in the SPS-LSS6 zone , which is used for the extraction of the beam to the LHC, and was placed on a mobile transfer table [8]. The table moved the cryomodule in the beamline for the CC tests and out of it for the usual SPS operation without breaking the vaccum. For the noise induced emittance growth studies only CC2 was used. Nevertheless, the parameters for both CCs are shown in Table 4.2 for completeness.
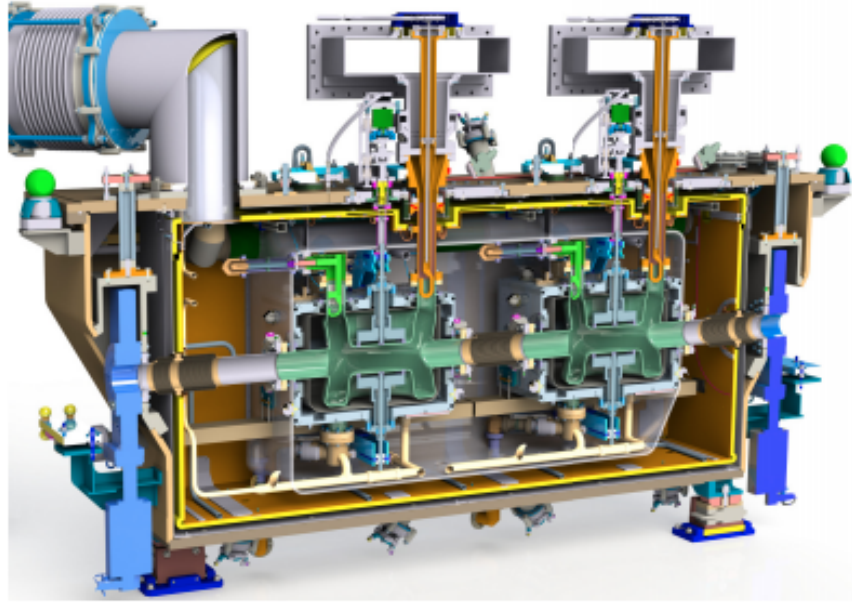
Figure 4.1: Cut of the CC cryomodule [7]. At its core there are the two DQW cavities, which are illustrated with light green color.

4.2.1 Operational considerations

For the beam tests with the CC in the SPS the approach regarding the energy ramp and the adjustment of the phasing with the main RF system needed to be evaluated and they are briefly discussed here.

Energy ramp

SPS recieves the proton beam at 26 GeV from the PS. It was found that the ramp to

Table 4.2: Crab cavities parameters for the emittance growth studies in SPS in 2018.

Parameter	Value	
	CC1	**CC2**
crabbing plane	vertical	vertical
s-location	6312.72 m	6313.32 m
CC voltage, V_{CC}	0 MV	1 MV
CC frequency, f_{CC}	400.78 MHz	400.78 MHz
Horizontal / Vertical beta function, $\beta_{x,CC}$ / $\beta_{y,CC}$	29.24 m / 76.07 m	30.31 m / 73.82 m
Horizontal / Vertical alpha function, $\alpha_{x,CC}$ / $\alpha_{y,CC}$	-0.88 m / 1.9 m	-0.91 m / 1.86 m
Horizontal / Vertical dispersion, $D_{x,CC}$ / $D_{y,CC}$	-0.48 m / 0 m	-0.5 m / 0 m

higher energies could not be performed with the CC on, as the beam was getting lost while crossing one of the vertical betatron sidebands due to resonant excitation [9]. Therefore, it was established that the acceleration has to be performed with the CC off and its voltage must be set up only after the energy of interest has been achieved. It is worth noting that this approach will also be used in the HL-LHC.

Crab Cavity - main RF synchronisation

It was important to ensure that during the "coast" the beam will epxeriene the same kick from the CC each turn. In other words the SPS main RF system operating at 200 MHz needed to be synchronous with the CC operating at 400 MHz. Due to the larger bandwidth of the SPS main RF system the CC was used as a master. Therefore the CC was operating at a fixed frequency and phase, while the main accelerating cavities were adjusted to the exact half of the CC frequency (see values at Tables 4.1 and 4.2) and were re-phased so that they become synchronous with the crabbing signal. For the studies at 270 GeV the synchronisation took place at the end of the ramp to the coast energy and shortly after the cavity was switched on [10].

4.3   SPS Head-Tail monitor

The Head-Tail (HT) monitor was the main diagnostic device deployed for the measurement of the crabbing and the calibration of the CC voltage. The HT moni-

tor was originally designed for measuring chromaticity and transverse isntabilities. Therefore its use as a crabbing diagnostic should be explained here. The methods and procedures described in this section were developed at CERN and they are described here for the completness of the thesis.

In the first part of this section some general information on the instrument along with example signals will be presented. Subsequently, the post processing of the HT signal in the presence of the CC will be discussed. Last, the calibration of the CC voltage from the HT data is described. The experimental data presented in this section were acquired at the SPS injection energy of 26 GeV with only one CC, CC1, at $\phi_{CC} = 0$ for simplicity. That energy of 26 GeV was chosen to provide a better understanding of the methods used as the orbit shift from the CC kick is stronger and thus more visible than in higher energies.

General information
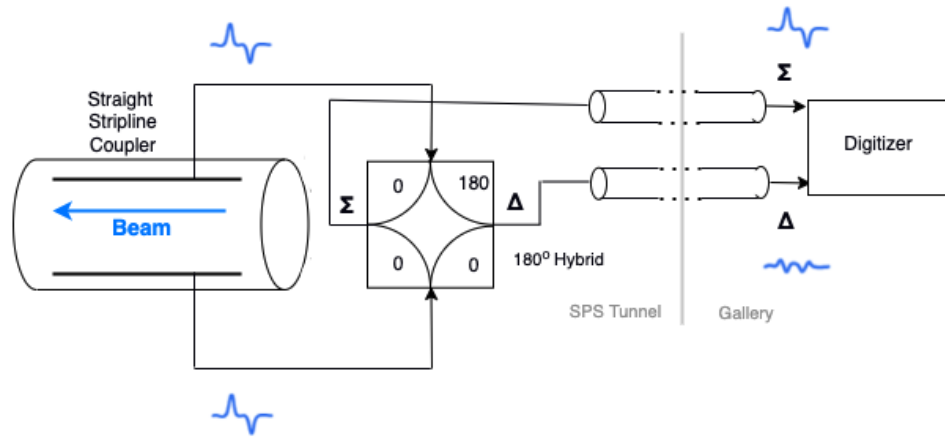
Figure 4.2: Diagram of the SPS HT monitor [11]. The beam is passing through a straight stripline coupler which is followed by a 180°hybrid. This configuration provides the sum and the difference signal of the two electrodes, which correspond to the longitudinal line desnity and intra-bunch offset, respectively.

The HT monitor is a high bandwidth version of a standard beam position monitor. The high bandwidth means that the monitor can measure the transverse offset within the bunch. This makes it ideal for the measurement of the intra-bunch offset caused from the CC kick. Its reading consists of the sum (Σ) and the difference (Δ)

of the electrode signals of a straight stripline coupler (Fig. 4.2) [12, 11] over a defined acquisition period. The sum signal is the longitudinal line density while the difference signal corresponds to the intra-bunch offset.

The raw signals from the HT monitor require a specific post-processing procedure, which is described in Ref. [11], in order to give useful information. Figure 4.3 shows some example signals obtained from the HT monitor after the basic post-processing is applied. Moreover, Fig. 4.4 shows a 2D representation of the HT monitor reading. It is worth noting here that in the specific example a clear modulating pattern in time of the vertical intra-bunch offset (vertical Δ) signal is observed. This is a result of the phase slip between the CC and the main RF system because they are not yet synchronised.
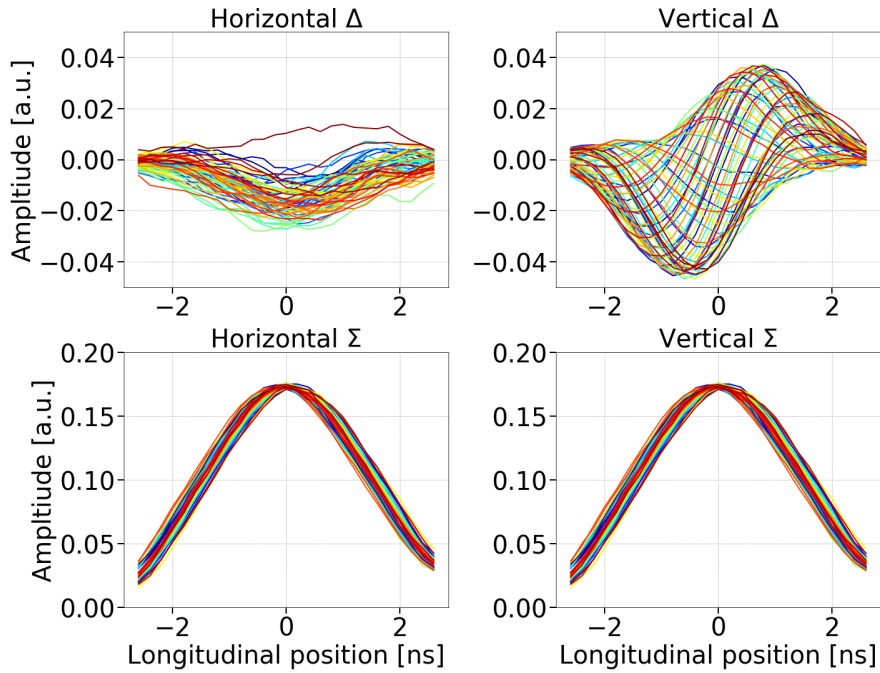
Figure 4.3: Example difference and sum signals (top and bottom plots, respectively) from the HT monitor with respect to the longitudinal position within the bunch over several SPS revolutions, after the basic post processing (Ref. [11]) but before the baseline correction. The different colors indicate the signals from different turns.

4.3.1 Post processing in the presence of Crab Cavities

To obtain useful information from the HT monitor signal in the presence of the CCs there are a few steps that differ from the standard post processing procedure and

Figure 4.4: 2D representation of example Δ and Σ signals with respect to the longitudinal position within the bunch obtained from the HT monitor over several SPS revolutions.

they are desribed below.

Heat-Tail monitor baseline correction

One issue of concern is the correction of the difference signal baseline due to orbit offsets and non-linearities of the instrument [11]. During the normal post processing, the correction is achieved by computing the mean of the difference signals over all turns and then subtracting this static offset from the signal of each turn. However, in the SPS tests, where the CCs are well synchronised with the main RF system (Section 4.2), the crabbing signal is also a static intra-bunch position offset and thus would also be removed with the usual method.

Therefore, for the CC experiments a reference measurement had first to be made with the CC unsynchronised. The mean of the Δ signal over this reference period was the baseline which then was subtracted from the Δ signals acquired after the synchronisation (Fig 4.5). The datasets before and after synchronisation are easily distinguishable in the 2D HT monitor reading as displayed in Fig. 4.6

Figure 4.5: HT monitor baseline correction for the SPS CC tests.

Figure 4.6: HT acquistions before and after the synchronisation of the SPS main RF with the CC.

Head-Tail monitor callibration

The last step to make the HT acquisitions meaningful is to convert the measured intra bunch offset, $\langle \Delta \rangle$, from arbitrary units to millimeters. The scaling is achieved by division with the $\langle \Sigma \rangle$ signal and with a normalisation factor which is provided by the calibration of the HT monitor [13]. The normalisation factor for the SPS was measured at 0.1052 in 2018 [14]. Figure 4.7 shows the intra-bunch offset from the CC kick in millimeters and after the baseline correction.

Figure 4.7: Intra-bunch offset from the CC kick expressed in millimeters after the removal of the baseline.

4.3.2 Crab Cavity voltage calibration

This section discusses the beam based measurement of the CC voltage from the HT monitor signal. The calibration was performed by using Eq. (4.1) to calculate the kick required to reconstruct the measured intra-bunch offset. Equation (4.1), which is obtained from Eq. (1) from chapter 4.7.1 in Ref. [15], gives the vertical orbit shift (in meters) from the CC kick, θ, at the HT monitor location as follows:

$$\Delta y_{,HT} = \frac{\sqrt{\beta_{y,HT}}}{2\sin(\pi Q_y)} \theta \sqrt{\beta_{y,CC}} \cos(\pi Q_y - |\psi_{y,HT} - \psi_{y,CC}|), \qquad (4.1)$$

where β_y is the beta function, Q_y is the tune, and $|\psi_{y,HT} - \psi_{y,CC}|$ between the CC and the HT monitor in tune units. The same applies for the horizontal plane. The subscripts HT and CC indicate quanities at the location of the HT monitor and CC respectively.

The deflection from the CC is written as $\theta = -\frac{qV(t)}{E_b}$, where q is the charge of the particle, E_b the beam energy and $V_{CC}(t) = V_{CC}\sin(2\pi f_{CC}t + \phi_{CC})$ is the voltage that a particle experiences while passing through the CC. In the context where the HT monitor measures the signal as a function of time, t, the voltage in the above formula is expressed accordingly as $V_{CC}(t)$, where $t = 0$ the center of the bunch.

It should be noted here, that the measured intra-bunch offset, $\Delta y_{,HT}$, is inserted in
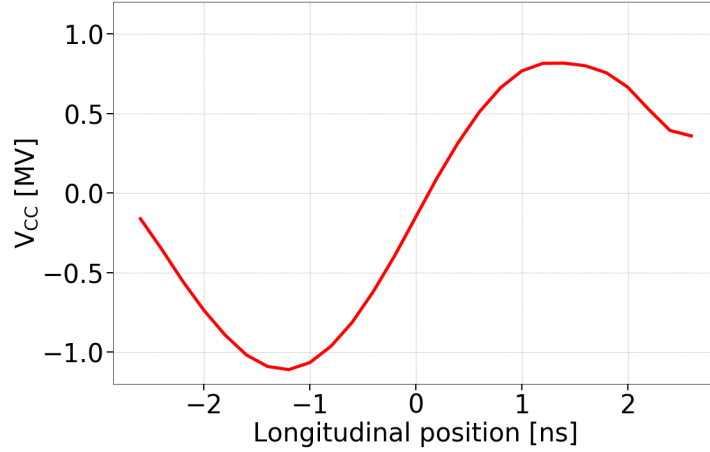
Figure 4.8: CC voltage calibration from the HT monitor.

Eq. (4.1) after removing the baseline and converting it to millimeters as discussed in Section 4.3.1. Figure 4.8 illustrates the cavity voltage computed from the HT signals shown already in this section. The corresponding beam and optic parameters are listed in Table 4.3.

Table 4.3: Parameters for computing the CC voltage from the example HT monitor measurements discussed in this chapter.

Parameter	Values
Beta function at the HT monitor, $\beta_{y,HT}$	49.19 m
Phase advance between the start of the lattice and the HT monitor, $\psi_{y,HT}$	$15.68 \times 2\pi$
Beta function at the CC1, $\beta_{y,CC1}$	76.07 m
Phase advance between the start of the lattice and CC1, $\psi_{y,CC1}$	$23.9 \times 2\pi$
Vertical betatron tune, Q_y	26.13
Beam energy, E_b	26 GeV

Reconstruction of crabbing

Additionally, the measurements from the HT monitor were used for reconstructing the crabbing and representating schematically the beam projection in the transverse plane. The technique for reconstructing the crabbing was developed at CERN in 2018 and was extensively used throught the experimental campaign with CCs since (together with the calibrated voltage) it gives a straightforward estimate of the applied CC kick, as illustrated in Fig. 4.9.

To obtain this schematic representation, which is practically a density plot, of the effect of the CC kick on the beam one needs to multiply the measured longitudinal profile, $\langle \Sigma \rangle$, with the measured intra-bunch offset (an example of this is shown in Fig. 4.7). For the transverse plane a gaussian distribution is considered with σ obtained from the wire scanner (addressed in more detail in the following section). The color code of Fig. 4.9 is normalised to the maximum intensity within the bunch.
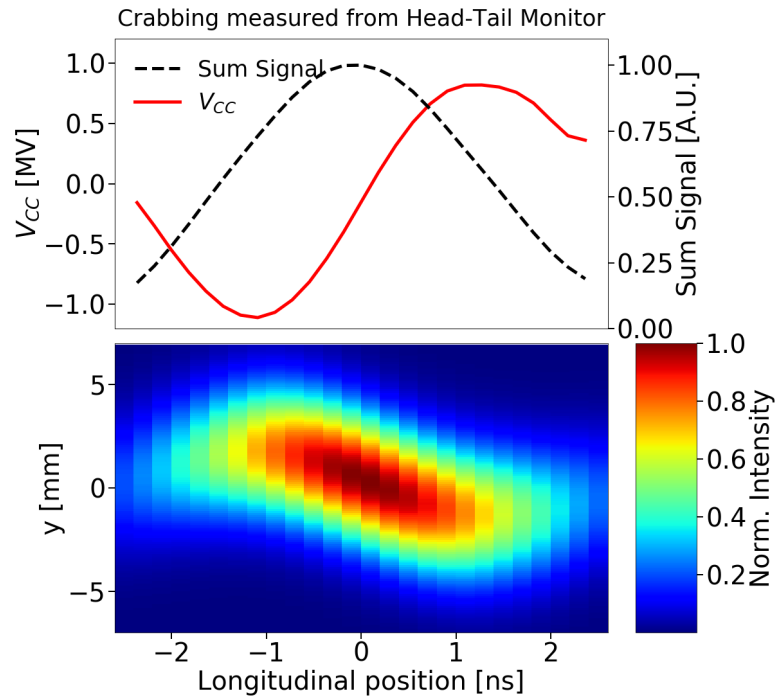
Figure 4.9: Illustration of the crabbing from the HT monitor signal. CC voltage and sum signal (longitudinal line density) measured from the HT monitor (top) together with the density plot (bottom) which visualises the effect of the CC kick in the beam.

4.4 SPS Wire Scanners

The SPS is equipped with Wire Scanners (WS) to measure the transverse beam emittance. The SPS WS system is described in detail in Ref. [16, 17]. For the SPS tests, the emittance was measured with WS both for the horizontal and vertical plane (BWS.51995.H and BWS.41677.V respectively).

The working principle is shown in Fig. 4.10. A thin wire rapidly moves across the

proton beam and a shower of secondary particles is generated. The signal from the secondary particles is then detected by a system of scintillator and photomultiplier (PM) detectors outside of the beam pipe. By measuring the PM current as a function of wire position over multiple turns the transverse beam profile is reconstructed. An example of a vertical profile is shown in Fig. 4.11.
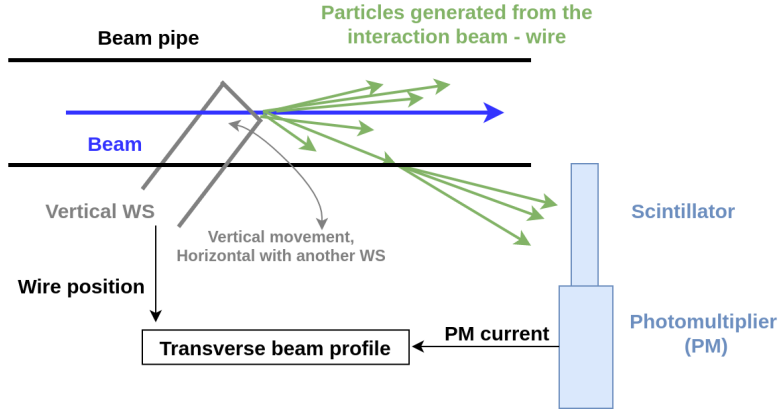
Figure 4.10: Sketch of the SPS rotational wire scanners [17]. The wire moves across the proton beam generating secondary particles which are then detecting by a scintillator and a photomultiplier. From the measured photomultiplier current the beam profile is reconstructed.

Fitting of transverse profiles

To obtain the beam size, σ, the transverse profiles from each scan are fitted with a four-parameter gaussian function:

$$f(x) = k + Ae^{-\frac{(x-\mu)^2}{2\sigma^2}}, \tag{4.2}$$

where k is the signal offset of the PM, A is the signal amplitude, μ is the mean of the Gaussian distribution and σ its standard deviation. The uncertainty of the measured beam size, $\Delta\sigma$, is defined as the one standard deviation error on σ which is computed from the square root of the diagonal elements of the covariant matrix.

The general formula for computing the normalised beam emittance from the beam size, σ is given by:

$$\epsilon = \frac{\sigma^2}{\beta_{WS}} \beta\gamma, \tag{4.3}$$

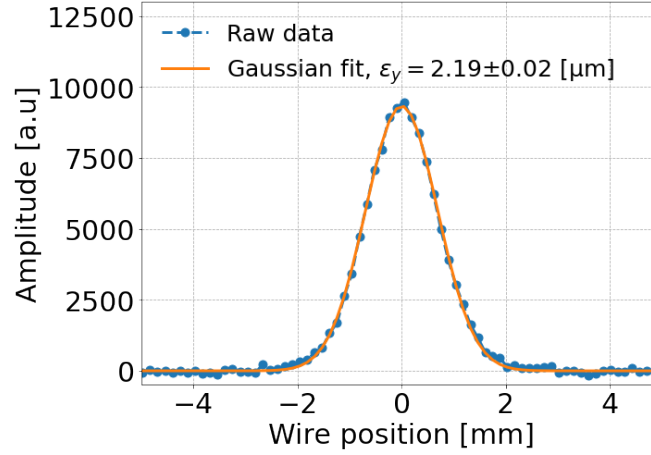Figure 4.11: Vertical beam profile obtained from the BWS.41677.V instrument. The measured data points (light blue) are fitted with a four parameter Gaussian (orange) to obtain the beam size. The calculated emittance is also shown.

where σ is the beam size, β_{WS} the beta function at the WS location and β, γ the relativistic parameters.

Note that, in the 2018 SPS operational configuration, the dispersion was small in the WSs location and thus its contribution to the beam size was considered to be negligible [1]. For the CC studies at 270 GeV beam energy, the beta functions were 81.5 m and 62.96 m at the locations of the horizontal and vertical WS respectively, while $\beta\gamma$ equals 287.8.

Assuming that the relativistic parameters and the beta fucntion are free of error, the uncertainty of the computed emittance, $\Delta\epsilon$, at a dispersion free region, depends only on the uncertainty of the measured beam size, $\Delta\sigma$, as:

$$\frac{\Delta\epsilon}{\epsilon} = \sqrt{\left(2\frac{\Delta\sigma}{\sigma}\right)^2} = 2\frac{\Delta\sigma}{\sigma}. \tag{4.4}$$

Further considerations

It is worth noting here that during each measurement with the WS the beam profile is actually acquired twice as the wire crosses the beam in the forward direction (IN

---

[1]The dispersion at BWS.51995.H location in 2018 was D_x= -15 mm. At 270 GeV, the energy spread, δ, is of the order of 10^{-4}. Thus, from Eq. (2.1) the horizontal normalised emittance from the dispersion is foreseen at the order of 10^{-11}. Comparing to the observed beam size during the CC tests of a few microns the dispersion is negligible

scan) and then in the reverse direction (OUT scan). For the 2018 measurements the emittance values obtained from IN and OUT scans, $\epsilon_{\text{IN}} \pm \Delta\epsilon_{\text{IN}}$ and $\epsilon OUT \pm \Delta\epsilon_{OUT}$,were found to be very similar. In the analysis of the 2018 measurements, the average emittance from the two scans, $\epsilon_{\text{avg}} = \langle\epsilon_{\text{IN}}, \epsilon_{\text{OUT}}\rangle$, is used. The uncertainty on the averaged emittance, $\Delta\epsilon_{\text{avg}}$, is computed as:

$$\Delta\epsilon_{avg} = \sqrt{\Delta\epsilon_1^2 + \Delta\epsilon_2^2}, \qquad (4.5)$$

where $\Delta\epsilon_1$ is the standard deviation of the ϵ_{IN} and ϵ_{OUT} and $\Delta\epsilon_2 = \sqrt{\langle\overline{\Delta\epsilon_{\text{IN}}, \Delta\epsilon_{\text{OUT}}}\rangle}$.

Finally, some emittance increase is expected during each wire scan, due to multiple Coulomb scattering. This effect has been extensively studied in Ref. [18]. For the rotational SPS WS and the energy of 270 GeV, at which the CC experiments were performed the expected emittance growth from the WS is expected to be small. However, a conservative number of scans were carried, $\sim$ 20 scans per bunch and per plane during $\sim$ 1 hour, in order to minimise the contribution from this effect.

4.5   ABWLM and Wall Current monitor

The bunch length was measured with two different instruments the ABWLM (A for RF, Beam, Wideband, Longitudinal, Measurement) [19] and the Wall Current monitor [20]. The ABWLM measures the longitudinal profiles from which the bunch length is computed by performing a gaussian fit. The Wall Current monitor acquirest not just the longitudinal profiles but also the longitudinal beam position relative to the monitor i.e. the beam arrival with respect to the reference. The bunch length is estimated by computing the full width half maximum of the profiles and then using it to estimate the sigma of a gaussian distribution. No further details on the operation of these instruments are discussed here as the offline analysis was not performed by the author.

5 | Experimental studies 2018: Measurements and analysis

1. present brifly the parameters 2. injected rf noise 3. MD emittance growth overview. - average from IN and OUT. As mentioned in CH4. vs time and vs noise level for all bunches. Not yet comparison with the theory. Probably you need to re-run this to make correctly the error propagation. - bunch length and longitudinal profiles and relative position from the wall current monitor. unstable bunches. - bunch 2-3-4 longutidinally unstable. - intensity –> no losses. 4. bunch 1 comparison with the theory. dey/dt vs noise levels plots. Factor of 4-5 difference.

5.1 Experimental procedure

Mention again briefly the experiemntal conditions, 1 vertical CC, 4 bunches, intensity 3e10 and chromaticity, Table 4.

5.2 Injected RF noise

In order to characterize the CC noise induced emittance growth, controlled noise was injected into their LLRF system and the evolution of the bunch was recorded for about 20-40 minutes. The injected noise was a mixture of amplitude and phase noise up to 10 KHz, overlapping and primarily exciting the fisrt betatron sideband at ~ 8 kHz. The phase noise was always dominant.

- Show 1 examples of AN and 1 of position, measured with a spectrum analyzer [Ref]

- effective noise - Comparison to the theroeical –> mention further explanation is

19

provided ip

5.3   Comparison with the theory

6 | Investigation of the discrepancy

6.1 Sensitvity studies

1. Sensitvity to how noisy is the noise spectrum 2. On the CC voltage 3. On the different bunch lengths.

6.2 b3b5b7 multiple errors

Contribution of the non-linearities with sixtracklib.

7 | Simple model of describing the decoherence suppression from impedance

8 | Application and impact for HL-LHC

9 | Conclusion

A | Appendix Title

Bibliography

[1]   P. Baudrenghien and T. Mastoridis. "Transverse emittance growth due to rf noise in the high-luminosity LHC crab cavities". In: *Phys. Rev. ST Accel. Beams* 18 (10 Oct. 2015), p. 101001. DOI: 10.1103/PhysRevSTAB.18.101001. URL: https://link.aps.org/doi/10.1103/PhysRevSTAB.18.101001.

[2]   R Calaga et al. "Proton-beam emittance growth in SPS coasts". In: *Conf. Proc.* C1205201 (May 2012), THPPP007. 3 p. URL: https://cds.cern.ch/record/1451286.

[3]   A Alekou et al. *Emittance growth in coast in the SPS*. Accessed: 26-11-2021. URL: https://indico.cern.ch/event/609486/contributions/2457542/attachments/1433340/2318716/EmittanceEvolutionCoastSPS_2017_April.pdf.

[4]   Fanouria Antoniou et al. "Emittance Growth in Coast in the SPS at CERN". In: *J. Phys.: Conf. Ser.* 1067 (2018), MOPMF061. 7 p. DOI: 10.18429/JACoW-IPAC2018-MOPMF061. URL: https://cds.cern.ch/record/2649815.

[5]   Michele Carlà et al. "Studies of a New Optics With Intermediate Transition Energy as Alternative for High Intensity LHC Beams in the CERN SPS". In: (2018), TUPAF022. 4 p. DOI: 10.18429/JACoW-IPAC2018-TUPAF022. URL: https://cds.cern.ch/record/2664976.

[6]   Androula Alekou et al. "SPS Long Term Stability Studies in the Presence of Crab Cavities and High Order Multipoles". In: (2018), WEP2PO008. 3 p. DOI: 10.18429/JACoW-HB2018-WEP2PO008. URL: https://cds.cern.ch/record/2640326.

[7]   C. Zanoni et al. "The crab cavities cryomodule for SPS test". In: 874 (July 2017), p. 012092. DOI: 10.1088/1742-6596/874/1/012092. URL: https://doi.org/10.1088/1742-6596/874/1/012092.

[8] Rama Calaga, Ofelia Capatina, and Giovanna Vandoni. "The SPS Tests of the HL-LHC Crab Cavities". In: (2018), TUPAF057. 4 p. DOI: 10.18429/JACoW-IPAC2018-TUPAF057. URL: https://cds.cern.ch/record/2649807.

[9] Rama Calaga. *SPS Crab Cavity test RF Test Program*. Accessed: 11-11-2021. URL: https://indico.cern.ch/event/718127/contributions/2951305/attachments/1645650/2629988/SPSCCtestv3.pdf.

[10] Carver Lee. *First proton beam dynamics results with crab cavities*. Accessed: 10-11-2021. URL: https://indico.cern.ch/event/800428/attachments/1804664/2945632/CrabCavity_BE_Seminar.pdf.

[11] Thomas Levens, Kacper Łasocha, and Thibaut Lefèvre. "Recent Developments for Instability Monitoring at the LHC". In: (2017), THAL02. 4 p. DOI: 10.18429/JACoW-IBIC2016-THAL02. URL: https://cds.cern.ch/record/2313358.

[12] R. Jones and H. Schmickler. "The measurement of Q' and Q" in the CERN-SPS by head-tail phase shift analysis". In: *PACS2001. Proceedings of the 2001 Particle Accelerator Conference (Cat. No.01CH37268)*. Vol. 1. 2001, 531–533 vol.1. DOI: 10.1109/PAC.2001.987561.

[13] T. E. Levens et al. "Automatic detection of transverse beam instabilities in the Large Hadron Collider". In: *Phys. Rev. Accel. Beams* 22 (11 Nov. 2019), p. 112803. DOI: 10.1103/PhysRevAccelBeams.22.112803. URL: https://link.aps.org/doi/10.1103/PhysRevAccelBeams.22.112803.

[14] Tom Levens. *Beam instrumentation with SPS Crabs*. Accessed: 11-11-2021. URL: https://indico.cern.ch/event/718127/contributions/2951309/attachments/1646050/2630808/BI_SPS_Crabs.pdf.

[15] Alexander Wu Chao et al. *Handbook of accelerator physics and engineering; 2nd ed.* Singapore: World Scientific, 2013. DOI: 10.1142/8543. URL: https://cds.cern.ch/record/1490001.

[16] J. Bosser et al. "Transverse emittance measurement with a rapid wire scanner at the CERN SPS". In: *Nuclear Instruments and Methods in Physics Research Section A: Accelerators, Spectrometers, Detectors and Associated Equipment* 235.3 (1985), pp. 475–480. ISSN: 0168-9002. DOI: https://doi.org/10.

1016/0168-9002(85)90096-8. URL: https://www.sciencedirect.com/science/article/pii/0168900285900968.

[17]   OE Berrig et al. *CERN-SPS Wire Scanner Impedance and Wire Heating Studies*. Tech. rep. Geneva: CERN, Sept. 2014. URL: https://cds.cern.ch/record/1972478.

[18]   Federico Roncarolo. "Accuracy of the Transverse Emittance Measurements of the CERN Large Hadron Collider". Presented 2005. 2005. URL: https://cds.cern.ch/record/1481835.

[19]   F. Follin G. Papotti. *Online bunch length measurement for SPS OP*. Accessed: 26-11-2021. URL: https://indico.cern.ch/event/774525/contributions/3218683/attachments/1756129/2847423/20181120_LIUSPSBD.pdf.

[20]   G Papotti. "A Beam Quality Monitor for LHC Beams in the SPS". In: (Sept. 2008), 4 p. URL: https://cds.cern.ch/record/1124099.